Dynamic regimes of random fuzzy logic networks



2011 New J. Phys. 13 013041

(http://iopscience.iop.org/1367-2630/13/1/013041)

New Journal of Physics
The open-access journal for physics

# Dynamic regimes of random fuzzy logic networks

**Dominik M Wittmann**[1] **and Fabian J Theis**

Computational Modeling in Biology, Institute for Bioinformatics and Systems Biology, Helmholtz Zentrum München—German Research Center for Environmental Health, Ingolstädter Landstrasse 1, 85764 Munich–Neuherberg, Germany
and
Centre for Mathematical Sciences, Technische Universität München, Boltzmannstrasse 3, 85748 Garching, Germany
E-mail: dominik.wittmann@helmholtz-muenchen.de

*New Journal of Physics* **13** (2011) 013041 (17pp)
Received 5 August 2010
Published 26 January 2011
Online at http://www.njp.org/
doi:10.1088/1367-2630/13/1/013041

**Abstract.** Random multistate networks, generalizations of the Boolean Kauffman networks, are generic models for complex systems of interacting agents. Depending on their mean connectivity, these networks exhibit ordered as well as chaotic behavior with a critical boundary separating both regimes. Typically, the nodes of these networks are assigned single discrete states. Here, we describe nodes by fuzzy numbers, i.e. vectors of degree-of-membership (DOM) functions specifying the degree to which the nodes are in each of their discrete states. This allows our models to deal with imprecision and uncertainties. Compatible update rules are constructed by expressing the update rules of the multistate network in terms of Boolean operators and generalizing them to fuzzy logic (FL) operators. The standard choice for these generalizations is the Gödel FL, where AND and OR are replaced by the minimum and maximum of two DOMs, respectively. In mean-field approximations we are able to analytically describe the percolation and asymptotic distribution of DOMs in random Gödel FL networks. This allows us to characterize the different dynamic regimes of random multistate networks in terms of FL. In a low-dimensional example, we provide explicit computations and validate our mean-field results by showing that they agree well with network simulations.

[1] Author to whom any correspondence should be addressed.

## Contents



## 1. Introduction

*Multistate models* (MMs) are a class of discrete dynamical systems. The model's variables take values in discrete, finite sets and develop in discrete time steps. At each time point, the value of a variable is determined by an *update rule* that deterministically depends upon the values of some of the other variables at the previous time point. MMs are frequently used to model molecular networks in theoretical biology [1]–[4]. In these applications, the discrete states of a variable are interpreted as, e.g., 'low'–'medium'–'high' or 'active'–'inactive', and the update rules are typically specified by propositional formulae (Boolean expressions), which often allow for an interpretation in terms of interacting regulatory mechanisms. For this reason, MMs are often referred to as *logical models*. (Here, we call them *crisp* logical models when confusion with the fuzzy logic (FL) models introduced below needs to be prevented.) Despite being a crude simplification of biological reality, logical modeling has become a popular tool in theoretical biology and has been substantiated from a biophysical [5] as well as a philosophical point of view [6].

In 1969, Kauffman proposed random MMs—the so-called *Kauffman networks* (KNs)—as generic models for large-scale gene regulatory networks [7]. Kauffman himself provided computational results in the special case of Boolean networks, where each variable assumes values either 'off' or 'on'. He showed that these networks exhibit surprisingly ordered structures and are able to give insights into biological phenomena such as cell replication or lineage differentiation. Interest in KNs was rekindled as their close relation to classical models from statistical mechanics was realized. In a number of studies [8]–[10], the self-organizing capacity of KNs was analyzed. It was shown that depending on their connectivity, KNs exhibit ordered as well as chaotic behavior with a critical boundary separating both regimes. The ordered

regime is characterized by small stable attractors, whereas in the chaotic regime long-periodic orbits frequently occur. These properties render both regimes unfavorable for the evolution of living organisms. Consequently, Kauffman promoted the idea of 'living at the edge of chaos' [11]. Interestingly, the critical connectivity of KNs is 2, which agrees well with the average connectivities of gene regulatory networks, e.g. in *Escherichia coli*, *Saccharomyces cerevisiae* and *Bacillus subtilis* [12]. These results about Boolean KNs can be extended straightforwardly to general random MMs [13, 14].

A major problem with MMs of molecular networks is the imprecision and subjectivity of categories such as 'high'–'low', 'active'–'inactive', etc. For this reason, FLs [15] are becoming an increasingly popular extension of logical models in theoretical biology. In an FL model, a variable is described by a *fuzzy number*, i.e. a vector of *degree-of-membership* (DOM) functions specifying the degree to which the variable is in each of its discrete states. Biological applications of FLs range from gene regulatory networks [16] over signal transduction and metabolic pathways [17]–[20] to ecological systems [21].

FL models are natural and biologically relevant generalizations of crisp logical models. However, they have not yet been combined with random KNs. This is what we address in this paper. We begin by recalling the phase transition criterion of multistate Kauffman networks (MKN) in section 2. In section 3, we then study FL versions of these networks. We briefly review the general concept of FLs and explain that FL models are, indeed, generalizations of crisp logical models. Subsequently, in section 4, we restrict ourselves to the *Gödel FL*, which can be distinguished from all other FLs as it can be derived from first principles. The dynamics of KNs with Gödel FL are described, and the observations are explained within a mean-field theory. Thus, a characterization of the three dynamic regimes of MKNs in terms of FL is obtained. We visualize our results by explicit computations in a low-dimensional example and further corroborate our findings by simulations of FL-KNs.

## 2. Phase transitions in random multistate networks

In this section, we review MKNs and briefly recall some results about critical phenomena; for a detailed account, see [14]. In the following, $\mathcal{G} = (V, E)$ will always denote a directed graph of order $N$ with nodes $V = \{1, 2, \ldots, N\}$ and edges $(i \to j) \in E \subset V \times V$. The ancestors (inputs) of a node $i$ are denoted by $i_1 < i_2 < \cdots < i_{K_i}$, where $K_i$ is the node's in-degree.

An *MM* is a triple $(\mathcal{G}, \mathcal{S}, \mathcal{F})$, which consists of a directed graph $\mathcal{G}$, a vector $\mathcal{S} = (S_i)_{i=1}^N$ of numbers of states defining the range $\Sigma_i := \{0, 1, \ldots, S_i - 1\}$ of node $i = 1, 2, \ldots, N$, and a vector of discrete functions $\mathcal{F} = (f_i)_{i=1}^N$, $f_i : \prod_{k=1}^{K_i} \Sigma_{i_k} \to \Sigma_i$. The discrete function $f_i$ is called *update rule* of node $i$. A *Boolean model* is the special case of an MM where all $S_i = 2$.

Each MM $(\mathcal{G}, \mathcal{S}, \mathcal{F})$ gives rise to a time-discrete dynamical system: with each node $i$ we associate a time-dependent discrete variable $x_i(t) \in \Sigma_i$, $X(t) = (x_i(t))_{i=1}^N$. The evolution of $X(t)$ is determined by the iteration

$$X(t+1) = \mathcal{F}(X(t)), \quad t = 0, 1, 2, \ldots,$$

where the $i$th component is given by

$$x_i(t+1) = f_i(x_{i_1}(t), x_{i_2}(t), \ldots, x_{i_{K_i}}(t)). \tag{1}$$

In this paper, we only consider the above synchronous updating, for different update policies, see e.g. [22, 23].

We now define MKNs generalizing the definition of KNs as given e.g. in [24]. An MKN is an MM where

(K1) the $K_i$ are chosen randomly from a probability distribution $P_{\text{in}}(K)$, $K = 1, 2, \ldots, K_{\max}$, $K_{\max} \leqslant N$;

(K2) the $K_i$ inputs $i_1, i_2, \ldots, i_{K_i}$ of $i$ are chosen randomly with uniform probability from among the network's nodes $1, 2, \ldots, N$;

(K3) the numbers of states $S_i$ are chosen randomly from a probability distribution $P_{\text{nos}}(S)$, $S = 2, 3, \ldots, S_{\max}$; and

(K4) the values of $f_i$ are chosen randomly from a probability distribution $P_{S_i}(s)$, $s \in \Sigma_i$.

Note that in (K4) the distribution $P_{S_i}$ does not depend on the node $i$ but only on its number of states $S_i$. In particular, in the Boolean case the update rules evaluate to 0 with a certain probability $w$ and to 1 with probability $1 - w$.

From (K4) it follows that the probability $p_{S_i}$ for the function $f_i$ to yield two different values for two different arguments depends only on $P_{S_i}$ and is given by

$$p_{S_i} = \sum_{s \in \Sigma_i} P_{S_i}(s)(1 - P_{S_i}(s)).$$

We define the first moment $\bar{p} = \sum_{S=2}^{S_{\max}} P_{\text{nos}}(S)\, p_S$ as well as the mean connectivity $\bar{K} = \sum_{K=1}^{K_{\max}} P_{\text{in}}(K)\, K$. In [14] it is shown that MKNs exhibit the following phase transition:

$$\bar{p}\bar{K} \begin{cases} < 1 & \text{ordered regime,} \\ = 1 & \text{critical boundary,} \\ > 1 & \text{chaotic regime.} \end{cases} \tag{2}$$

## 3. Fuzzy logic Kauffman networks

In this section, we consider again MKNs as introduced in section 2. However, now we use FLs to evaluate the network. For the sake of clarity, we denote the variables of the FL model by $\tilde{x}_i(t)$, $i = 1, 2, \ldots, N$. The variable $\tilde{x}_i(t)$ is no longer assigned exactly one value from $\Sigma_i$. Rather its state at time $t$ is given by a vector

$$\tilde{x}_i(t) = \begin{pmatrix} \tilde{x}_i^0(t) \\ \tilde{x}_i^1(t) \\ \vdots \\ \tilde{x}_i^{S_i-1}(t) \end{pmatrix}$$

of DOM functions $\tilde{x}_i^s(t) \in [0, 1]$ indicating the degree to which $\tilde{x}_i(t)$ has states $s \in \Sigma_i$. Note that we do not require any normalization of $\tilde{x}_i(t)$.

In crisp logic, update rule (1) can be written as

$$x_i(t+1) = s \quad \Longleftrightarrow \quad \bigvee_{(\xi_1, \xi_2, \ldots, \xi_{K_i}) \mid f_i(\xi_1, \xi_2, \ldots, \xi_{K_i}) = s} \; \bigwedge_{k=1}^{K_i} \left( x_{i_k}(t) = \xi_k \right), \tag{3}$$

$s \in \Sigma_i$. The disjunction (OR-gate) on the right-hand side runs over all arguments of $f_i$ with output value $s$. For each argument, the inner conjunction (AND-gate) is true if and only if the argument agrees with the input values at time $t$. Now that variables are assigned fuzzy numbers, the Boolean equations $x_i(t+1) = s$ and $x_{i_k}(t) = \xi_k$ from this update rule no longer assume crisp *true–false* values, but their degrees of truth are given by the DOMs $\tilde{x}_i^s(t+1) \in [0, 1]$ and $\tilde{x}_{i_k}^{\xi_k}(t) \in [0, 1]$, respectively. We therefore need to generalize the Boolean operators AND, OR and NOT to the unit interval.

### *3.1. A short primer on fuzzy logic*

Let us now briefly introduce these generalizations of the Boolean operators; for details, see [25]. The generalized NOT operator is a *strong negation*, i.e. a function $\neg : [0, 1] \to [0, 1]$ satisfying

(N1) $\neg(0) = 1$ and $\neg(1) = 0$,
(N2) $\neg$ is continuous and strictly decreasing,
(N3) $\neg$ is an involution, $\neg(\neg(x)) = x$.

For the generalization of AND and OR, one typically uses the concepts of *t-norms* and *t-conorms*. AND is replaced by a t-norm, i.e. by a function $\top : [0, 1] \times [0, 1] \to [0, 1]$ satisfying

(T1) $\top(x, \top(y, z)) = \top(\top(x, y), z)$,
(T2) $\top(x, y) = \top(y, x)$,
(T3) $\top(x, y) \leqslant \top(x', y')$ if $x \leqslant x'$ and $y \leqslant y'$,
(T4) $\top(x, 1) = x$.

Analogously, an OR is replaced by a t-conorm, i.e. by a function $\top : [0, 1] \times [0, 1] \to [0, 1]$ satisfying (T1)–(T3) and

(T4′) $\top(x, 0) = x$.

Clearly, for non-fuzzy DOMs, i.e. DOMs either 0 or 1, the above definitions reduce to their standard versions. We remark that, for fixed $\neg$, t-norms and t-conorms are dual concepts under a generalized DeMorgan's law: with every t-norm $\top$ we can associate a dual t-conorm $\perp$ via

$$\perp(x, y) = \neg\left(\top\left(\neg(x), \neg(y)\right)\right).$$

(T1) allows us to inductively define the t-norm and t-conorm of more than two arguments.

It is impossible for a dual pair of t-norm and t-conorm to preserve all laws from Boolean algebra. In fact, there is a trade-off between the classical *Aristotelian laws of thought*—the law of the excluded middle and the law of non-contradiction—on the one hand, and the distributive law, the law of absorption and idempotency on the other hand. It can be shown that any law of the latter group is respected only by the Gödel t-norm and t-conorm $\top(x, y) = \min(x, y)$ and $\perp(x, y) = \max(x, y)$, which are dual under the negation $\neg(x) = 1 - x$, cf appendix A. These choices of t-norm and t-conorm, in turn, violate both the law of the excluded middle and the law of non-contradiction. These properties allow us to deduce the Gödel pair from first principles [26] and make it the standard choice.

### 3.2. General fuzzy logic Kauffman networks

We generalize update rule (3) to the FL update rule

$$\tilde{x}_i^s(t+1) = \perp(\top(\tilde{x}_{i_1}^{\xi_1}(t), \ldots, \tilde{x}_{i_{K_i}}^{\xi_{K_i}}(t)) | f_i(\xi_1, \ldots, \xi_{K_i}) = s), \tag{4}$$

$s \in \Sigma_i$. These update rules define a function $\tilde{\mathcal{F}}$ mapping a state $\tilde{X}(t) = (\tilde{x}_1(t), \tilde{x}_2(t), \ldots, \tilde{x}_N(t))$ onto its successor $\tilde{X}(t+1) = (\tilde{x}_1(t+1), \tilde{x}_2(t+1), \ldots, \tilde{x}_N(t+1))$.

Let us conclude this section by showing that (4) is, indeed, a generalization of update rule (3). To this end, consider non-fuzzy states, i.e. states $\tilde{X}(t)$ where for all $i$ there exists $s_i$ such that $\tilde{x}_i^{s_i}(t) = 1$ and $\tilde{x}_i^s(t) = 0$, $s \neq s_i$. There is a canonical bijection $\phi$ between the states $X(t)$ and the non-fuzzy states $\tilde{X}(t)$. Clearly, $\phi$ is compatible with the mappings $\mathcal{F}$ and $\tilde{\mathcal{F}}$ in the sense that for a non-fuzzy state $\tilde{X}(t)$ also $\tilde{X}(t+1) = \tilde{\mathcal{F}}(\tilde{X}(t))$ is non-fuzzy and the diagram

$$\begin{array}{ccc} \prod_{i=1}^N \Sigma_i & \xrightarrow{\phi} & \phi\left(\prod_{i=1}^N \Sigma_i\right) \\ \Big\downarrow{\scriptstyle \mathcal{F}} & & \Big\downarrow{\scriptstyle \tilde{\mathcal{F}}} \\ \prod_{i=1}^N \Sigma_i & \xrightarrow{\phi} & \phi\left(\prod_{i=1}^N \Sigma_i\right) \end{array}$$

commutes.

## 4. Kauffman networks with Gödel fuzzy logic

In this section, we treat the special case of the Gödel t-norm and t-conorm. We concretize update rule (4) accordingly and obtain

$$\tilde{x}_i^s(t+1) = \max_{(\xi_1,\xi_2,\ldots,\xi_{K_i}) | f_i(\xi_1,\xi_2,\ldots,\xi_{K_i})=s} \left( \min_{k=1}^{K_i} \left( \tilde{x}_{i_k}^{\xi_k}(t) \right) \right), \quad s \in \Sigma_i. \tag{5}$$

Let us see how this update rule works in a simple example.

**Example 4.1** *Consider the part of a network shown in figure 1. Node $i$ has $S_i = 4$ discrete states and $K_i = 2$ inputs $i_1$ and $i_2$ with $S_{i_1} = 3$ and $S_{i_2} = 2$ states, respectively. The figure also shows the truth-table of the update rule $f_i$. We assume that at time $t$ the states of the nodes $i_1$ and $i_2$ are given by the vectors of DOMs $\tilde{x}_{i_1}(t) = (0.7, 0.3, 0.4)$ and $\tilde{x}_{i_2}(t) = (0.2, 0.8)$. Then, following (5), we compute the state of node $i$ at time $t+1$ as*

$$\begin{aligned} \tilde{x}_i^0(t+1) &= \max_{(\xi_1,\xi_2) | f_i(\xi_1,\xi_2)=0} (\min(\tilde{x}_{i_1}^{\xi_1}(t), \tilde{x}_{i_2}^{\xi_2}(t))) \\ &= \max(\min(\tilde{x}_{i_1}^1(t), \tilde{x}_{i_2}^0(t)), \min(\tilde{x}_{i_1}^2(t), \tilde{x}_{i_2}^1(t))) \\ &= \max(\min(0.3, 0.2), \min(0.4, 0.8)) = 0.4, \\ \tilde{x}_i^1(t+1) &= \max(\min(0.3, 0.8)) = 0.3, \\ \tilde{x}_i^2(t+1) &= \max(\min(0.7, 0.2)) = 0.2, \\ \tilde{x}_i^3(t+1) &= \max(\min(0.4, 0.2), \min(0.7, 0.8)) = 0.7\,. \end{aligned}$$

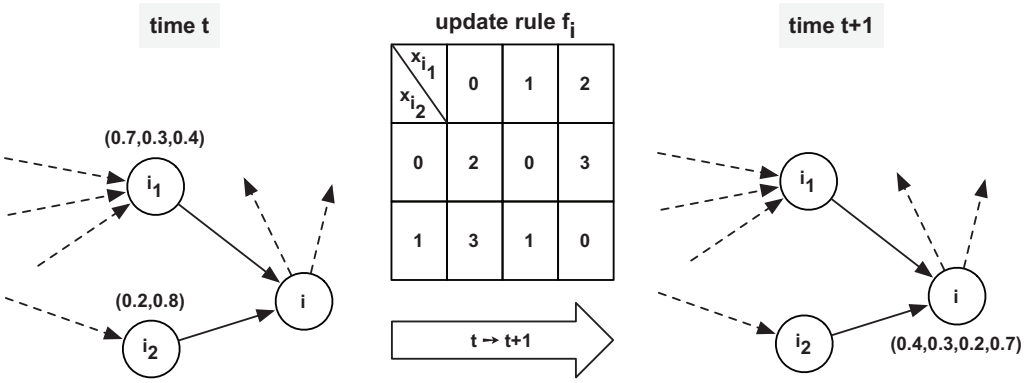


**Figure 1.** The left and right columns show the neighborhood of some node $i$ in a network at times $t$ and $t+1$, respectively. Node $i$ has $S_i = 4$ discrete states and $K_i = 2$ inputs $i_1$ and $i_2$ with $S_{i_1} = 3$ and $S_{i_2} = 2$ states. At time $t$ the states of nodes $i_1$ and $i_2$ are given by the vectors of DOMs $\tilde{x}_{i_1}(t) = (0.7, 0.3, 0.4)$ and $\tilde{x}_{i_2}(t) = (0.2, 0.8)$. In the middle column, the truth-table of the update rule $f_i$ is shown. Together with (5), $f_i$ implies $\tilde{x}_i(t+1) = (0.4, 0.3, 0.2, 0.7)$, see example 4.1 for the computations.

### *4.1. Phenomenology*

We begin by phenomenologically describing the dynamics of KNs with Gödel FL. To this end, we sample three networks containing $N = 10^4$ nodes, each with $S = 3$ states and $K = 2$ inputs, i.e. $P_{\text{nos}}(S) = \delta_{S,2}$ and $P_{\text{in}}(K) = \delta_{K,2}$. The entries of the update rules are sampled from the three distributions:

$$\begin{aligned} &P_3^{(a)}(0) = 3/4, \quad P_3^{(a)}(1) = 1/8, \quad P_3^{(a)}(2) = 1/8, \\ &P_3^{(b)}(0) = 2/3, \quad P_3^{(b)}(1) = 1/6, \quad P_3^{(b)}(2) = 1/6 \quad \text{and} \\ &P_3^{(c)}(0) = 1/2, \quad P_3^{(c)}(1) = 1/4, \quad P_3^{(c)}(2) = 1/4. \end{aligned} \tag{6}$$

One easily computes $\bar{p}^{(a)}\bar{K} = 13/32 \times 2 = 26/32$, $\bar{p}^{(b)}\bar{K} = 1/2 \times 2 = 1$ and $\bar{p}^{(c)}\bar{K} = 5/8 \times 2 = 5/4$. Thus, according to (2) the three networks fall into the frozen, critical and chaotic regimes.

Initial DOMs are drawn randomly from a uniform probability distribution on [0, 1] and the networks are evolved for 20 time steps. The histograms in figures 2(A)–(C) show the distributions of the DOMs in the three networks over time. In each subfigure, the DOMs are, of course, evenly distributed across the unit interval at time $t = 0$. We observe that in each network the range of the DOMs sharply decreases over time until, finally, all DOMs fall into a few bins at the lower end of the unit interval. At $t = 20$, the distributions of DOMs have reached a steady state in each network. These steady-state distributions differ between the three networks, cf the insets in figures 2(A)–(C). In each case, DOMs are divided into two bins. However, whereas in the frozen network shown in (A) only about one-third of the DOMs end up in the higher bin, this bin contains almost all DOMs of the chaotic network shown in (C). In the critical network from (B), the two bins are approximately evenly populated. Simulations with different realizations (not shown) produce similar results. We now give an explanation for these observations in a mean-field approximation of FL-KNs.

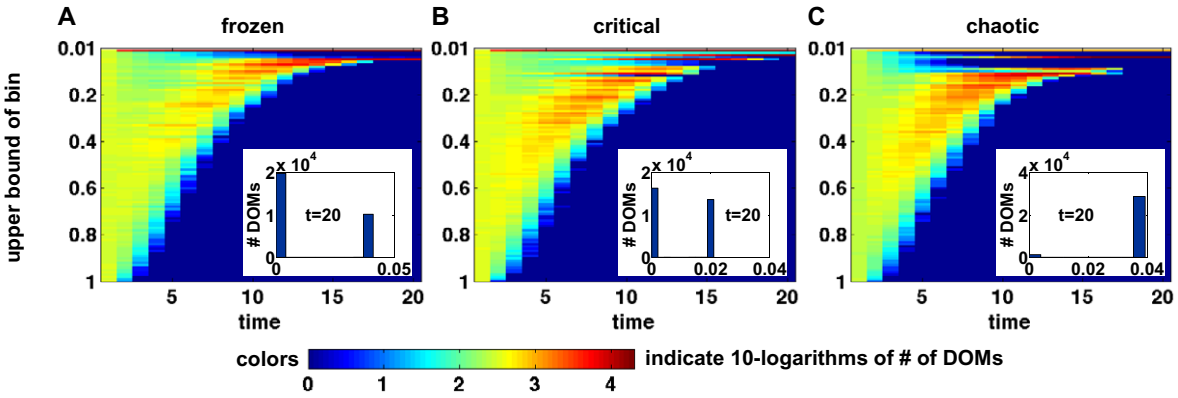


**Figure 2.** Simulations of three networks with $N = 10^4$, $P_{\text{nos}}(S) = \delta_{S,3}$, $P_{\text{in}}(K) = \delta_{K,2}$ and (A) $P_3^{(a)}$, (B) $P_3^{(b)}$, (C) $P_3^{(c)}$ from (6). As derived in the main text, the three networks fall into the (A) frozen, (B) critical and (C) chaotic regimes. For each network, initial DOMs are drawn randomly from a uniform probability distribution on the unit interval and the network is simulated for 20 time steps according to update rule (5). Each subfigure shows the distributions of the DOMs over time. At $t = 20$ this distribution has reached a steady state in each network. For visualization, the unit interval is subdivided into 100 equally sized bins, whose upper bounds are shown on the $y$-axis. Colors indicate the 10-logarithm of the number of DOMs in the respective bin, cf the colorbar shown above. Note that there is a total of $\bar{S} \cdot N = 3 \times 10^4$ DOMs. The insets in panels (A)–(C) show the steady-state distributions of the DOMs at time $t = 20$. In each case, DOMs are divided into two bins. The ratios of high and low DOMs, however, differ greatly between frozen, critical and chaotic networks.

### *4.2. Bounds for degrees-of-membership*

First we turn our attention to the decreasing range of the DOMs. More precisely, we show that the DOMs become bounded by the smallest maximal DOM per node at time $t = 0$, which we denote by $m$. Formally,

$$m := \min_{i=1}^{N} \max_{s \in \Sigma_i} \tilde{x}_i^s(0). \tag{7}$$

If $N$ is large and the initial conditions are sampled uniformly, we may expect $m$ to be small. Thus, this upper bound indeed explains the observed decrease of the DOMs. We call a node $i$ *bounded at time* $t$ if it satisfies

$$\max_{s \in \Sigma_i} \tilde{x}_i^s(t) = m. \tag{8}$$

Clearly, for random initial DOMs, exactly one node is bounded at $t = 0$; we denote it by $\bar{i}$.

Now let us consider an FL-KN with general $P_{\text{in}}$, $P_{\text{nos}}$ and $P_S$ in the thermodynamic limit $N \to \infty$. To understand the long-term behavior of the quantity

$$b(t) := \frac{1}{N} \cdot \#\{i \,|\, i \text{ is bounded at time } t.\}$$

we set up an iteration $b(t+1) = H(b(t))$ in a mean-field approximation. To this end, consider some node $i$ at time $t+1$. We show that node $i$ will be bounded at $t+1$ if and only if any of its inputs is bounded at time $t$. First, suppose that $i$ has an input, w.l.o.g. $i_1$, which is bounded at $t$. Then $m$ is an upper bound on the DOMs $\tilde{x}_i^s(t+1)$. Moreover, for $(\xi_1, \xi_2, \ldots, \xi_{K_i})$ satisfying $\tilde{x}_{i_k}^{\xi_k}(t) = \max_{s\in\Sigma_{i_k}} \tilde{x}_{i_k}^s(t) \geqslant m$, $k = 1, 2, \ldots, K_i$, we have $\min_{k=1}^{K_i} \tilde{x}_{i_k}^{\xi_k}(t) = m$ and, hence, $\tilde{x}_i^{f_i(\xi_1,\xi_2,\ldots,\xi_{K_i})}(t+1) = m$. Conversely, assume that none of $i$'s inputs are bounded at $t$ and let $(\xi_1, \xi_2, \ldots, \xi_{K_i})$ again be defined as above. Now this implies $\min_{k=1}^{K_i} \tilde{x}_{i_k}^{\xi_k}(t) > m$ and, hence, $\tilde{x}_i^{f_i(\xi_1,\xi_2,\ldots,\xi_{K_i})}(t+1) > m$.

Because, in the thermodynamic limit, the inputs of $i$ can be assumed to be independent [27], we may write

$$b(t+1) = H\left(b(t)\right) := \sum_{K=1}^{K_{\max}} P_{\text{in}}(K)\left[1 - (1 - b(t))^K\right].$$

Note that this is the mean probability that at least one input of a node is bounded at $t$. In the two fixed points $b^\star = 1$ and $b^{\star\star} = 0$ of this iteration, we have $H'(b^\star) = P_{\text{in}}(1)$ and $H'(b^{\star\star}) = \bar{K}$, respectively. From $\bar{K} > 1 \Longleftrightarrow P_{\text{in}}(1) < 1$ it follows that, if $\bar{K} > 1$, the fixed point $b^\star = 1$ is stable and the fixed point $b^{\star\star} = 0$ is unstable. Hence, for $\bar{K} > 1$, the network will ultimately reach a state where all nodes are bounded. Visually speaking, if $\bar{K} > 1$, property (8) percolates through the network. Emanating from node $\bar{i}$, at each time step all nodes satisfying this property bequeath it to their descendants.

### *4.3. Distributions of degrees-of-membership*

Let us now explain the observed differences in the steady-state distributions between the three dynamic regimes. For this, we restrict ourselves to the special case $P_{\text{nos}}(S) = \delta_{S,\bar{S}}$ and study the behavior for $\bar{K} > 1$ in more detail, so let $\bar{K} > 1$. We may then assume that each DOM $\tilde{x}_i^s(t) \leqslant m$ and that at least one DOM per node is equal to $m$ after some time $t_0$. We study the distribution $Z(t) = (Z^z(t))_{z=0}^{\bar{S}}$,

$$Z^z(t) := \frac{1}{N} \cdot \#\{i \,|\, \tilde{x}_i(t) \text{ has } z \text{ DOMs equal to } m\}, \quad z = 0, \ldots, \bar{S}, \tag{9}$$

of DOMs $m$ per node in the network. In this section, we will consider only times $t \geqslant t_0$. Hence, we have $Z^0(t) = 0$ and may thus omit this component.

Our goal now is to set up an iteration $Z(t+1) = E(Z(t))$ for this distribution in a mean-field approximation. To this end, let us consider some node $i$ at time $t+1$. We describe its inputs by a vector $(\kappa_1, \kappa_2, \ldots, \kappa_{\bar{S}})$ indicating the number of inputs with $1, 2, \ldots, \bar{S}$ DOMs $m$ at time $t$. Clearly, $\kappa_1 + \kappa_2 + \cdots + \kappa_{\bar{S}} = K_i$. In the thermodynamic limit, we may assume the inputs to be independent [27] and the probability for the configuration $(\kappa_\zeta)_{\zeta=1}^{\bar{S}}$ is given by

$$\binom{K_i}{\kappa_1, \ldots, \kappa_{\bar{S}}} \prod_{\zeta=1}^{\bar{S}} \left(Z^\zeta(t)\right)^{\kappa_\zeta}.$$

The number of tuples $(\xi_1, \xi_2, \ldots, \xi_{K_i})$ satisfying $\tilde{x}_{i_k}^{\xi_k}(t) = m$, $k = 1, 2, \ldots, K_i$, is $\prod_{\zeta=1}^{\bar{S}} \zeta^{\kappa_\zeta}$. The $\tilde{x}_i^{f_i(\xi_1,\xi_2,\ldots,\xi_{K_i})}(t+1)$ belonging to these tuples are the DOMs of $\tilde{x}_i(t+1)$ which are equal to $m$.

To compute their number, we let $\ell(\zeta, z)$ denote the probability that $\zeta$ fields, which are randomly filled with numbers $0, 1, \ldots, \bar{S}-1$ according to $P_{\bar{S}}$, contain exactly $z$ different elements. For notational convenience, we let $\ell(\prod_{\zeta=1}^{\bar{S}} \zeta^{\kappa_\zeta}, z) = \ell((\kappa_\zeta), z)$. The $\ell(\zeta, z)$ are difficult to compute analytically and one has to resort to exhaustive enumeration. We can, however, make use of the following relations.

**Lemma 4.1**

*(i) For any $\bar{S}$ and $P_{\bar{S}}$ we have $\ell(1,1) > \ell(2,2) > \cdots > \ell\left(\bar{S}, \bar{S}\right)$.*

*(ii) For $\bar{S} = 3$ and any $P_3$ we have $\ell(2,2) \leqslant \ell(3,2)$.*

*(iii) For any $\bar{S}$ and $P_{\bar{S}}$ we have $\ell\,(1,1) \geqslant \ell\,(2,1) \geqslant \cdots \geqslant \ell\left(\bar{S}, 1\right)$ with equalities if and only if $P_{\bar{S}}$ is a degenerate delta-distribution.*

We are now able to set up an iteration for the probabilities $Z(t)$ in a mean-field approximation:

$$Z(t+1) = E(Z(t)), \tag{10}$$

where the $z$th component $E^z(Z(t))$ of the right-hand side is given by

$$\sum_{K=1}^{K_{\max}} P_{\text{in}}\,(K) \sum_{\kappa_1+\cdots+\kappa_{\bar{S}}=K} \binom{K}{\kappa_1, \ldots, \kappa_{\bar{S}}} \prod_{\zeta=1}^{\bar{S}} (Z^\zeta(t))^{\kappa_\zeta} \cdot \ell((\kappa_\zeta), z).$$

It is intuitive and can also easily be shown that $Z^\star = (1, 0, \ldots, 0)^t$ is a fixed point of this iteration. We now investigate its stability. The distributions $Z(t)$ live on the affine hyperplane of $\mathbb{R}^{\bar{S}}$ defined by $\sum_{z=1}^{\bar{S}} Z^z(t) = 1$. In order to take derivatives, we think of it as a manifold and choose as a global chart the projection on the first $\bar{S}-1$ coordinates. We remark that the choice of charts, in general, does affect the Jacobian, but not its eigenvalues, as a change of charts merely means a change of basis in the tangent space. Hence, this choice is not crucial for stability analyses. The Jacobian of $E$ at $Z^\star$ can be written in global coordinates as

$$J = \mathrm{D}E|_{Z_\star} = \bar{K} \cdot \left[ \begin{pmatrix} \ell\,(1,1) & \ell\,(2,1) & \cdots & \ell\left(\bar{S}-1, 1\right) \\ 0 & \ell\,(2,2) & \cdots & \ell\left(\bar{S}-1, 2\right) \\ \vdots & \vdots & \ddots & \vdots \\ 0 & 0 & \cdots & \ell\left(\bar{S}-1, \bar{S}-1\right) \end{pmatrix} \right.$$
$$\left. - \begin{pmatrix} \ell\left(\bar{S}, 1\right) & \ell\left(\bar{S}, 1\right) & \cdots & \ell\left(\bar{S}, 1\right) \\ \ell\left(\bar{S}, 2\right) & \ell\left(\bar{S}, 2\right) & \cdots & \ell\left(\bar{S}, 2\right) \\ \vdots & \vdots & \ddots & \vdots \\ \ell\left(\bar{S}, \bar{S}-1\right) & \ell\left(\bar{S}, \bar{S}-1\right) & \cdots & \ell\left(\bar{S}, \bar{S}-1\right) \end{pmatrix} \right], \tag{11}$$

cf appendix B. It can be shown that the eigenvalues of $J$ are $\bar{K} \cdot \ell\,(s, s)$, $s = 2, 3, \ldots, \bar{S}$, cf appendix C. From lemma 4.1 it follows that the largest eigenvalue is $\bar{K} \cdot \ell\,(2,2)$. Further note that $\ell\,(2,2) = \sum_{s=0}^{\bar{S}-1} P_{\bar{S}}(s)(1 - P_{\bar{S}}(s)) = p_{\bar{S}} = \bar{p}$. Thus, in terms of FL, the dynamic regimes of

MKNs from (2) have the following characteristics:

**$\bar{K} = 1$ :** Property (8) does not percolate through the entire network.

**$\bar{K} > 1$ and $\bar{p}\bar{K} < 1$ :** Eventually, all nodes satisfy (8). The state where only one DOM per node is equal to $m$ is stable.

**$\bar{K} > 1$ and $\bar{p}\bar{K} = 1$ :** Critical boundary.

**$\bar{K} > 1$ and $\bar{p}\bar{K} > 1$ :** Eventually, all nodes satisfy (8). The state where only one DOM per node is equal to $m$ is unstable.

Iteration (10) is exact in the thermodynamic limit from time $t_0$ on. Recall that this is the time after which each DOM $\tilde{x}_i^s(t) \leqslant m$ and at least one DOM per node is equal to $m$. The crucial point is whether $Z(t_0) = Z^\star$ or not. If yes, it follows that $Z(t) = Z^\star$ for all $t > t_0$ as $Z^\star$ is a fixed point. In this case its stability is irrelevant. If not, the differences between the dynamic regimes come into play. In the frozen regime, the fixed point $Z^\star$ is attractive and we may expect $Z(t) = Z^\star$ at some point in time. In the chaotic regime, $Z^\star$ is repellent.

Let us now see which case occurs if we draw the initial DOMs randomly from a uniform probability distribution on [0, 1]. To this end, consider the update of a node $i$ with input node $\bar{\imath}$, w.l.o.g. $\bar{\imath} = i_1$. As the initial DOMs are uniformly distributed, each input $i_k$, $k = 2, 3, \ldots, K_i$, has expected $\bar{S}(1-m)$ DOMs bigger than $m$ at $t = 0$. Moreover, for sufficiently large $N$, we have $m \ll 1$, and consequently $\bar{S}(1-m) > 1$. Hence, we expect at least $(\bar{S}(1-m))^{K_i - 1} \gg 1$ different tuples $(\xi_1, \xi_2, \ldots, \xi_{K_i})$ such that $\min_{k=1}^{K_i} \tilde{x}_{i_k}^{\xi_k}(0) = m$. Consequently, also the expected number of DOMs $\tilde{x}_i^s(1)$ that are set to $m$ will be greater than 1. Inductively, this shows that $Z(t_0) \neq Z^\star$. We have thus found an explanation for the observed differences between the dynamic regimes in section 4.1. In the following, these differences are analyzed in more detail.

### *4.4. Example and network simulations*

We finish by detailing the behavior of the distributions $Z(t)$ in a specific example, more precisely in the case $\bar{S} = 3$. The distribution $P_3$ will be assumed to be non-degenerate, i.e. $P_3(s) \neq 1$ for $s = 0, 1, 2$. In particular, we address the following questions:

(i) Are the global dynamics in the frozen regime governed by the stable fixed point $Z^\star$?

(ii) What is the asymptotic behavior in the chaotic regime?

Again, we work in the projection of (10) on the first two coordinates

$$\begin{pmatrix} Z^1(t+1) \\ Z^2(t+1) \end{pmatrix} = \begin{pmatrix} E^1\left(Z^1(t), Z^2(t)\right) \\ E^2\left(Z^1(t), Z^2(t)\right) \end{pmatrix}.$$

The implicit function theorem guarantees the existence of maps $Z_1^2(Z^1)$ and $Z_2^2(Z^1)$ around $Z^\star$ satisfying $E^1(Z^1, Z_1^2(Z^1)) = Z^1$ and $E^2(Z^1, Z_2^2(Z^1)) = Z^2$, respectively. Together with (11) this theorem also implies

$$\frac{\mathrm{d}Z_1^2}{\mathrm{d}Z^1}(1) = -\frac{\bar{K}\left[\ell(1,1) - \ell(3,1)\right] - 1}{\bar{K}\left[\ell(2,1) - \ell(3,1)\right]} \tag{12}$$

$$\frac{\mathrm{d}Z_2^2}{\mathrm{d}Z^1}(1) = -\frac{-\bar{K}\,\ell(3,2)}{\bar{K}\left[\ell(2,2) - \ell(3,2)\right] - 1}. \tag{13}$$

**Table 1.** Coefficients $c_i$ for equations (14) and (15).

| | |
|---|---|
| $c_1 = \ell(1,1) - 2\ell(3,1) + \ell(9,1)$ | $c_2 = 2\ell(2,1) - 2\ell(3,1) - 2\ell(6,1) + 2\ell(9,1)$ |
| $c_3 = \ell(4,1) - 2\ell(6,1) + \ell(9,1)$ | $c_4 = 2\ell(3,1) - 2\ell(9,1)$ |
| $c_5 = 2\ell(6,1) - 2\ell(9,1)$ | $c_6 = \ell(9,1)$ |
| $c_7 = \ell(1,2) - 2\ell(3,2) + \ell(9,2)$ | $c_8 = 2\ell(2,2) - 2\ell(3,2) - 2\ell(6,2) + 2\ell(9,2)$ |
| $c_9 = \ell(4,2) - 2\ell(6,2) + \ell(9,2)$ | $c_{10} = 2\ell(3,2) - 2\ell(9,2)$ |
| $c_{11} = 2\ell(6,2) - 2\ell(9,2)$ | $c_{12} = \ell(9,2)$ |

First observe that lemma 4.1 implies $\mathrm{d}Z_2^2/\mathrm{d}Z^1(1) < 0$. In appendix D, it is shown that the dynamic regimes of MKNs from (2) have the following characteristics:

$$\bar{\boldsymbol{p}}\bar{\boldsymbol{K}} < \mathbf{1}: \frac{\mathrm{d}Z_1^2}{\mathrm{d}Z^1}(1) > -1, \quad \frac{\mathrm{d}Z_2^2}{\mathrm{d}Z^1}(1) > -1,$$

$$\bar{\boldsymbol{p}}\bar{\boldsymbol{K}} = \mathbf{1}: \frac{\mathrm{d}Z_1^2}{\mathrm{d}Z^1}(1) = -1, \quad \frac{\mathrm{d}Z_2^2}{\mathrm{d}Z^1}(1) = -1,$$

$$\bar{\boldsymbol{p}}\bar{\boldsymbol{K}} > \mathbf{1}: \frac{\mathrm{d}Z_1^2}{\mathrm{d}Z^1}(1) < -1, \quad \frac{\mathrm{d}Z_2^2}{\mathrm{d}Z^1}(1) < -1.$$

Let us now visualize this for $P_{\mathrm{in}}(K) = \delta_{K,2}$. Here, we can easily compute

$$Z_1^2(Z^1) = \frac{-c_5 - c_2 Z^1 + \sqrt{(c_5 + c_2 Z^1)^2 - 4c_3(c_6 - Z^1 + c_4 Z^1 + c_1 (Z^1)^2)}}{2c_3} \tag{14}$$

and

$$Z_2^2(Z^1) = \frac{1 - c_{11} - c_8 Z^1 - \sqrt{(-1 + c_{11} + c_8 Z^1)^2 - 4c_9(c_{12} + c_{10} Z^1 + c_7 (Z^1)^2)}}{2c_9} \tag{15}$$

with coefficients $c_i$ from table 1. Figures 3(A)–(C) show $Z_1^2(Z^1)$ and $Z_2^2(Z^1)$ from (14) and (15), respectively, for the three distributions $P_3^{(a/b/c)}$ from (6), which fall into the frozen, critical and chaotic regimes. Whereas in the frozen and critical regimes (cf figures 3(A) and (B)) $Z^\star$ is the only fixed point, an additional (stable) fixed point $Z^{\star\star}$ emerges in the chaotic regime (cf figure 3(C)).

We now further investigate these situations by simulations of FL-KNs. Figures 3(D)–(F) show the distributions $Z(t) = (Z^z(t))_{z=0}^3$ in simulations of FL-KNs for the same choices of $P_3$ as in figures 3(A)–(C). First of all, we observe the percolation of property (8) through the network as in each case $Z^0(t)$ (yellow bars) decreases over time. Moreover, we detect nice agreement between the coordinates of the (attractive) fixed points in panels (A)–(C) and the steady-state distributions in panels (D)–(F). The agreement is worst between panels (B) and (E) due to the critical fixed point. (For numerical details see the figure caption.) With respect to our initiatory questions, we observe that the asymptotic dynamics in the frozen regime are, indeed, governed by the stable fixed point $Z^\star$ and that the asymptotic dynamics in the chaotic regime are governed by the additional attractive fixed point $Z^{\star\star}$.

This result also explains our findings in section 4.1. Here, we observed that in the frozen regime, finally about one-third of all DOMs are equal to $m$, cf figure 2(A). This agrees with the fact that in the stable steady-state $Z^\star$ only one out of $\bar{S} = 3$ DOMs per node is equal to $m$. In the chaotic regime, almost all DOMs were found to be ultimately equal to $m$, cf figure 2(C). Accordingly, in the stable steady state $Z^{\star\star}$ about 70% of all nodes have three DOMs equal to $m$ and a further 27% of all nodes have two DOMs equal to $m$.

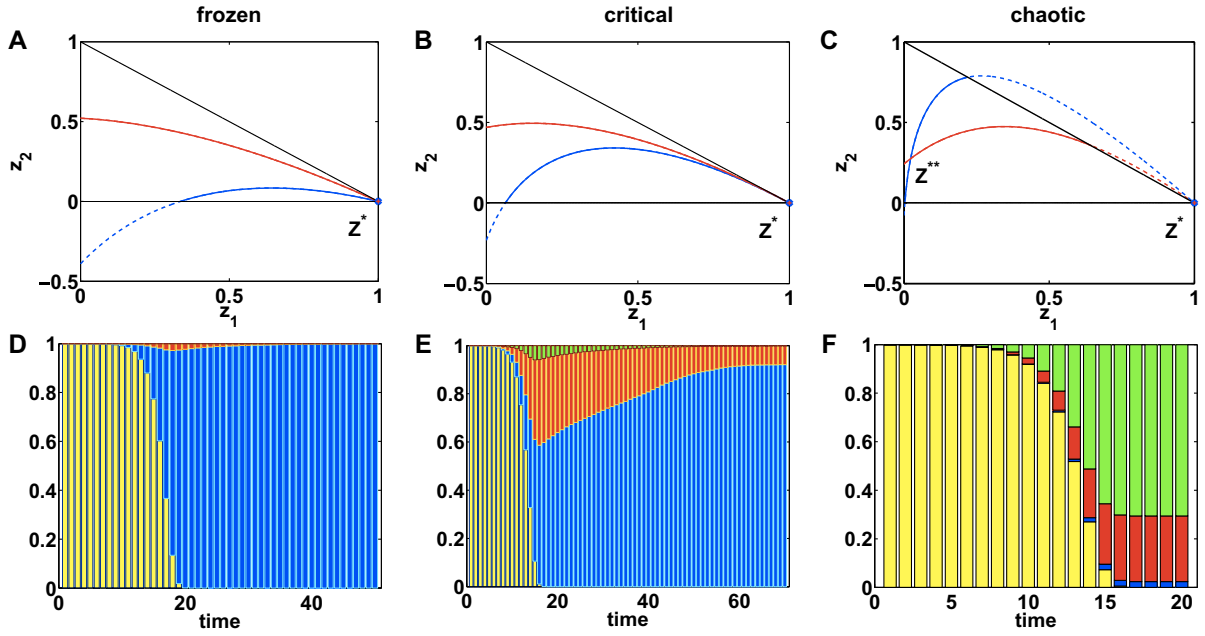


**Figure 3.** The situation of delta-distributed $S$ and $K$ at $\bar{S} = 3$ and $\bar{K} = 2$. Panels (A)–(C) show $Z_1^2(Z^1)$ (blue) and $Z_2^2(Z^1)$ (red) from (14) and (15), respectively, for (A) $P_3^{(a)}$, (B) $P_3^{(b)}$ and (C) $P_3^{(c)}$ from (6). The coordinates of the fixed points are $Z^\star = (1, 0)$ and in (C) $Z^{\star\star} \approx (0.0226, 0.2747)$. Panels (D)–(F) show the distributions $Z(t) = (Z^z(t))_{z=0}^3$ in simulations of FL-KNs with $N = 10^4$ nodes and $P_3$ as in (A)–(C). According to (9), $Z^z(t)$ was computed as the fraction of nodes with $z$ DOMs equal to $m$, where $m = \min_{i=1}^N \max_{s\in\Sigma_i} \tilde{x}_i^s(0)$. Color legend: $Z^0(t)$: yellow; $Z^1(t)$: blue; $Z^2(t)$: red; and $Z^3(t)$: green. The final distributions are (D) $Z(60) = (0, 0.9993, 0.0007, 0)^t$, (E) $Z(70) = (0, 0.9207, 0.0765, 0.0028)^t$ and (F) $Z(20) = (0, 0.0235, 0.2708, 0.7057)^t$. These steady-state distributions agree well with the coordinates of the (attractive) fixed points in panels (A)–(C). Abbreviations: FL, fuzzy logic; KN, Kauffman network.

## 5. Conclusions

In this paper, we studied FL-KNs. These are random MMs, where nodes are described by fuzzy numbers, i.e. vectors of DOM functions specifying the degree to which the nodes are in each of their discrete states. The update rules are constructed by replacing the Boolean operators AND and OR by continuous generalizations, the so-called t-norms and t-conorms.

We first observed that, for any choice of t-norm and t-conorm, an FL model is a true generalization of the underlying crisp model in the sense that for non-fuzzy initial conditions the behavior of the latter is reproduced. Subsequently, Gödel FL-KNs were studied in more detail. We found that, unless the mean connectivity equals one, the DOM $m$ from (7) (the smallest of the maximal DOMs per node) percolates through the network, i.e. $m$ becomes a global upper bound for all DOMs in the network.

One can interpret $m$ as the maximal amount of uncertainty present in the network. Node $\bar{i}$ (the node whose maximal DOM is equal to $m$ at $t = 0$) is the node that we have the greatest

difficult assigning a discrete state to. For $\bar{K} > 1$ this maximal uncertainty $m$ becomes a global bound on the certainties with which we assign to nodes their discrete states.

How many DOMs per node are equal to $m$ depends on the dynamic regime of the MKN. More precisely, we could analytically show in a mean-field approximation that the state where only one DOM per node is equal to $m$ is stable in frozen networks and unstable in chaotic networks. In a low-dimensional example, we explicitly computed the distribution of DOMs $m$ and could show that the results from our mean-field approximations well agree with simulations of FL-KNs.

The differences in the behavior of the DOMs in the different regimes have significant dynamical consequences. Let us first consider a frozen MKN and assume that at time $t$ only one of the DOMs $\tilde{x}_i(t)$ of node $i$ is equal to $m$ for all $i = 1, 2, \ldots, N$. We define $s_i \in \Sigma_i$ such that $\tilde{x}_i^{s_i}(t) = m$ and initialize the crisp MKN by setting $x_i(t)$ equal to $s_i$, $i = 1, 2, \ldots, N$. After evolving the crisp MKN for one time step, $x_i(t+1)$ indicates the state of node $i$ whose DOM is equal to $m$ at time $t+1$ in the FL-KN, i.e. $\tilde{x}_i^{x_i(t+1)}(t+1) = m$. Hence, the dynamics of the FL-KN are strongly related to the dynamics of the crisp MKN. This is no longer the case for chaotic MKNs. Here, the FL-KN ultimately reaches a state where a large fraction of DOMs are equal to $m$. Consequently, the dynamics of the FL-KN contains no information about the dynamics of the crisp MKN.

Future work could address the behavior of other FLs, such as the probabilistic or Łukasiewicz FL. From a more general point of view, FL models are an intermediate between discrete and continuous models. They are fully specified by a discrete model but allow (discrete-)time evolutions of a continuous state space. It would be interesting to compare this to other continuous extensions of logical models as proposed e.g. in [28, 29].

## Acknowledgments

DMW thanks Florian Blöchl (Helmholtz Center Munich) for a critical reading of the manuscript, useful discussions and stimulating remarks. The Helmholtz Alliance on Systems Biology (project 'CoReNe') is gratefully acknowledged for funding this work.

## Appendix A

It can be verified by straightforward computations that the Gödel t-norm and -conorm are indeed idempotent and satisfy the distributive law and the law of absorption. To show uniqueness, we first prove that the Gödel t-(co)norm is the only idempotent t-(co)norm. So, suppose that we are given a pair $(\top, \bot)$ of dual t-norm and t-conorm satisfying $\top(x, x) = x$ and $\bot(x, x) = x$ for all $x \in [0, 1]$. Further, let $x, y \in [0, 1]$, w.l.o.g. $x \leqslant y$. Then, $x = \top(x, 1) \geqslant \top(x, y) \geqslant \top(x, x) = x$ and, hence, $\top(x, y) = x = \min(x, y)$. From the duality of $(\top, \bot)$ it follows that $\bot(x, y) = \max(x, y)$.

We continue by proving that each distributive pair $(\top, \bot)$ of dual t-norm and t-conorm is idempotent and, thus, the Gödel-pair. Assuming distributivity, it holds for $x \in [0, 1]$

$$\begin{aligned} x &= \top(x, 1) \geqslant \top(x, \bot(1, 1)) \\ &= \bot(\top(x, 1), \top(x, 1)) = \bot(x, x) \geqslant \bot(x, 0) = x. \end{aligned}$$

It follows that $\bot(x, x) = x$ and from the duality of $(\top, \bot)$ also $\top(x, x) = x$.

It remains to be shown that each pair $(\top, \perp)$ of dual t-norm and t-conorm, which satisfies the law of absorption, is idempotent and, thus, the Gödel-pair. For such $(\top, \perp)$ and $x \in [0, 1]$ it holds $x = \top(x, \perp(x, 0)) = \top(x, x)$. Again, duality implies $\perp(x, x) = x$.

## Appendix B

Let us first consider the case of fixed $K$. In global coordinates we can write

$$E^z(Z^1, \ldots, Z^{\bar{S}-1}) = \sum_{\kappa_1+\cdots+\kappa_{\bar{S}}=K} \binom{K}{\kappa_1, \ldots, \kappa_{\bar{S}}} \prod_{\zeta=1}^{\bar{S}-1} (Z^\zeta)^{\kappa_\zeta} \left(1 - \sum_{\zeta=1}^{\bar{S}-1} Z^\zeta\right)^{\kappa_{\bar{S}}} \ell((\kappa_\zeta), z).$$

Differentiating with respect to $Z^s$ yields

$$\frac{\mathrm{d}E^z}{\mathrm{d}Z^s} = \sum_{\kappa_1+\cdots+\kappa_{\bar{S}}=K} \binom{K}{\kappa_1, \ldots, \kappa_{\bar{S}}} \ell((\kappa_\zeta), z) \times \prod_{\zeta \neq s, \bar{S}} \left(Z^\zeta\right)^{\kappa_\zeta} \left[ -(Z^s)^{\kappa_s} \kappa_{\bar{S}} \left(1 - \sum_{\zeta=1}^{\bar{S}-1} Z^\zeta\right)^{\kappa_{\bar{S}}-1} + \kappa_s (Z^s)^{\kappa_s-1} \left(1 - \sum_{\zeta=1}^{\bar{S}-1} Z^\zeta\right)^{\kappa_{\bar{S}}} \right],$$

where, formally, $0 \times 0^{-1} = 0$. The evaluation of this term at $Z^\star$ is

$$\left.\frac{\mathrm{d}E^z}{\mathrm{d}Z^s}\right|_{Z^\star} = K \cdot \ell(s, z) - K \cdot \ell(\bar{S}, z).$$

To see this, note that the only non-zero contributions to the sum over the $(\kappa_1, \ldots, \kappa_{\bar{S}})$ are the combinations $(K, 0, \ldots, 0, 0)$ and $(K-1, 0, \ldots, 0, 1)$ if $s = 1$, and the combinations $\kappa_1 = K-1, \ldots, \kappa_s = 1, \ldots, \kappa_{\bar{S}} = 0$ and $\kappa_1 = K-1, \ldots, \kappa_s = 0, \ldots, \kappa_{\bar{S}} = 1$ if $s \neq 1$.

For general $P_{\mathrm{in}}$ the linearity of the derivative implies

$$\left.\frac{\mathrm{d}E^z}{\mathrm{d}Z^s}\right|_{Z^\star} = \sum_{K=1}^{K_{\max}} P_{\mathrm{in}}(K)\, K[\ell(s, z) - \ell(\bar{S}, z)] = \bar{K}[\ell(s, z) - \ell(\bar{S}, z)].$$

## Appendix C

According to (11), we write $J = \bar{K}(A - B)$ with $(\bar{S}-1) \times (\bar{S}-1)$ matrices $A$ and $B$. We extend $A$ to an $\bar{S} \times \bar{S}$ upper triangular matrix $A'$ by an $\bar{S}$th row $(0, 0, \ldots, \ell(\bar{S}, \bar{S}))$ and $\bar{S}$th column $\mathfrak{a} = (\ell(\bar{S}, 1), \ell(\bar{S}, 2), \ldots, \ell(\bar{S}, \bar{S}))^t$. For $s = 2, 3, \ldots, \bar{S}$ let $v_s = (v_s^r)_{r=1}^{\bar{S}}$ be an eigenvector to the eigenvalue $\ell(s, s)$ of $A'$. As $A'$ is a left stochastic matrix, it follows from $\ell(s, s) v_s = A v_s$ that $\ell(s, s) \sum_{r=1}^{\bar{S}} v_s^r = \sum_{r=1}^{\bar{S}} v_s^r$. Thus, $\sum_{r=1}^{\bar{S}} v_s^r = 0$, since $\ell(s, s) < 1$. As $B$ consists of identical columns $\mathfrak{a}$ this implies $B(v_s^r)_{r=1}^{\bar{S}-1} = -v_s^{\bar{S}} \mathfrak{a}$. It follows that

$$(A - B)(v_s^r)_{r=1}^{\bar{S}-1} = \ell(s, s)(v_s^r)_{r=1}^{\bar{S}-1} - v_s^{\bar{S}} \mathfrak{a} + v_s^{\bar{S}} \mathfrak{a} = \ell(s, s)(v_s^r)_{r=1}^{\bar{S}-1},$$

which shows that $\bar{K}\ell(s, s)$ is an eigenvalue of $J$.

## Appendix D

To determine the relation between the nominator and the denominator in (12) and (13), we compute

$$\begin{aligned}
&\bar{K}\left[\ell\left(1,1\right)-\ell\left(3,1\right)\right]-1-\bar{K}\left[\ell\left(2,1\right)-\ell\left(3,1\right)\right]\\
&\quad=\bar{K}\left[\ell\left(1,1\right)-\ell\left(3,1\right)-\ell\left(2,1\right)+\ell\left(3,1\right)\right]-1\\
&\quad=\bar{K}\left[1-\ell\left(2,1\right)\right]-1\\
&\quad=\bar{K}\,\ell\left(2,2\right)-1
\end{aligned}$$

and

$$\begin{aligned}
&-\bar{K}\,\ell\left(3,2\right)-\bar{K}\left[\ell\left(2,2\right)-\ell\left(3,2\right)\right]+1\\
&\quad=\bar{K}\left[-\ell\left(3,2\right)-\ell\left(2,2\right)+\ell\left(3,2\right)\right]+1\\
&\quad=1-\bar{K}\,\ell\left(2,2\right).
\end{aligned}$$

Recall that $\ell(2,2)=\bar{p}$. To obtain the claim, consider that according to lemma 4.1 the denominators in (12) and (13) are positive and negative, respectively.

## References


[1] Thomas R 1991 Regulatory networks seen as asynchronous automata: a logical description. *J. Theor. Biol.* **153** 1–23

[2] Sánchez L and Thieffry D 2001 A logical analysis of the Drosophila gap-gene system *J. Theor. Biol.* **211** 115–41

[3] Fauré A, Naldi A, Lopez F, Chaouiya C, Ciliberto A and Thieffry D 2009 Modular logical modelling of the budding yeast cell cycle *Mol. BioSyst.* **5** 1787–96

[4] Wittmann D M, Blöchl F, Trümbach D, Wurst W, Prakash N and Theis F J 2009 Spatial analysis of expression patterns predicts genetic interactions at the mid-hindbrain boundary *PLoS Comput. Biol.* **5** e1000569

[5] Buchler N E, Gerland U and Hwa T 2003 On schemes of combinatorial transcription logic *Proc. Natl Acad. Sci. USA* **100** 5136–41

[6] Isalan M and Morrison M 2009 This title is false *Nature* **458** 969

[7] Kauffman S A 1969 Metabolic stability and epigenesis in randomly constructed genetic nets *J. Theor. Biol.* **22** 437–67

[8] Derrida B and Pomeau Y 1986 Random networks of automata: a simple annealed approximation *Europhys. Lett.* **1** 45–9

[9] Derrida B and Stauffer D 1986 Phase transitions in two dimensional Kauffman cellular automata *Europhys. Lett.* **2** 739–45

[10] Flyvbjerg H 1988 An order parameter for networks of automata *J. Phys. A: Math. Gen.* **21** L955–60

[11] Kauffman S A 1993 *The Origins of Order: Self-Organization and Selection in Evolution* (Oxford: Oxford University Press)

[12] Balleza E, Alvarez-Buylla E R, Chaos A, Kauffman S A, Shmulevich I and Aldana M 2008 Critical dynamics in genetic regulatory networks: examples from four kingdoms *PLoS One* **3** e2456

[13] Solé R V, Luque B and Kauffman S A 2000 Phase transitions in random networks with multiple states *Working Papers 00-02-011* Santa Fe Institute

[14] Wittmann D M, Marr C and Theis F J 2010 Biologically meaningful update rules increase the critical connectivity of generalized Kauffman networks *J. Theor. Biol.* **266** 436–48

[15] Zadeh L A 1965 Fuzzy sets *Inf. Control* **8** 338–53

[16] Woolf P J and Wang Y 2000 A fuzzy logic approach to analyzing gene expression data *Physiol. Genomics* **3** 9–15
[17] Windhager L and Zimmer R 2008 Intuitive modeling of dynamic systems with Petri nets and fuzzy logic *German Conf. on Bioinformatics* vol 136GI pp 106–15
[18] Franco-Lara E and Weuster-Botz D 2007 Application of fuzzy-logic models for metabolic control analysis *J. Theor. Biol.* **245** 391–9
[19] Aldridge B B, Saez-Rodriguez J, Muhlich J L, Sorger P K and Lauffenburger D A 2009 Fuzzy logic analysis of kinase pathway crosstalk in TNF/EGF/insulin-induced signaling *PLoS Comput. Biol.* **5** e1000340
[20] Kriete A, Bosl W J and Booker G 2010 Rule-based cell systems model of aging using feedback loop motifs mediated by stress responses *PLoS Comput. Biol.* **6** e1000820
[21] Meesters E H, Bak R P M, Westmacott S, Ridgley M and Dollar S 1998 A fuzzy logic model to predict coral reef development under nutrient and sediment stress *Conserv. Biol.* **12** 957–65
[22] Chavez M, Albert R and Sontag E 2005 Robustness and fragility of Boolean models for genetic regulatory networks *J. Theor. Biol.* **235** 431–49
[23] Greil F, Drossel B and Sattler J 2007 Critical Kauffman networks under deterministic asynchronous update *New J. Phys.* **9** 373
[24] Aldana M, Coppersmith S and Kadanoff L P 2003 Boolean dynamics with random couplings *Perspectives and Problems in Nonlinear Science: A Celebratory Volume in Honor of Lawrence Sirovich* (Berlin: Springer) pp 23–89
[25] Fodor J 2004 Left-continuous t-norms in fuzzy logic: an overview *Acta Polytech. Hung.* **1** 141–56
[26] Bellman R and Giertz M 1973 On the analytic formalism of the theory of fuzzy sets *Inf. Sci.* **5** 149–56
[27] Hilhorst H J and Nijmeijer M 1987 On the approach of the stationary state in Kauffman's random Boolean network *J. Physique* **48** 185–91
[28] Plahte E, Mestl T and Omholt S W 1998 A methodological basis for description and analysis of systems with complex switch-like interactions *J. Math. Biol.* **36** 321–48
[29] Wittmann D M, Krumsiek J, Saez-Rodriguez J, Lauffenburger D A, Klamt S and Theis F J 2009 Transforming Boolean models to continuous models: methodology and application to T-cell receptor signaling *BMC Syst. Biol.* **3** 98